ARTICLE

Chiral Mesophases of Hydrogen-bonded Liquid Crystals

Florian Malotke,[a†] Marco Saccone,[ab†] Christoph Wölper,[c] Ronald Y. Dong,[d] Carl A. Michal,[d] and Michael Giese*[a]

Received 00th January 20xx,
Accepted 00th January 20xx

DOI: 10.1039/x0xx00000x

The chiral induction in hydrogen-bonded liquid crystals is investigated. The experimental study was accompanied by detailed density functional theory calculations and variable-temperature solid-state deuteron NMR measurements indicating that interactions between the linking groups of the hydrogen-bond accepting unit play a key role in the chiral induction.

Introduction

The induction of chirality into liquid crystals is a promising route towards the development of photonic materials for application in sensing and optical devices.[1–4] Cholesteric liquid crystals (CLCs = chiral-nematic liquid crystals, N*) represent one-dimensional (1D) photonic band gap materials, which selectively reflect circularly polarised light of one handedness according to Bragg's law, when the helical pitch is on the order of the wavelength of visible light.

Blue phases (BPs) are closely related chiral mesophases, which occur in a narrow temperature range between the isotropic (I) and chiral nematic (N*) phases. They represent double-twisted superstructures with three-dimensional (3D) periodic cubic lattices (BPI and BPII, Figure 1)[5] and are induced by chiral dopants with high helical twisting powers (HTP).[6]

Due to the dynamic nature of the liquid crystalline state photonic structures based on CLCs or BPs can be used for the design of responsive photonic materials or sensors.[1,4,7] In general, chiral mesophases are derived from mixing nematic liquid crystalline hosts (e.g. 4-Cyano-4'-alkylbiphenyls, *n*CB) with a chiral dopant.[8] Since most reported systems consist of a complex composition of mesogens, chiral dopants and further additives it is challenging to ensure the compatibility of all components in order to prevent phase separation.[8–10]

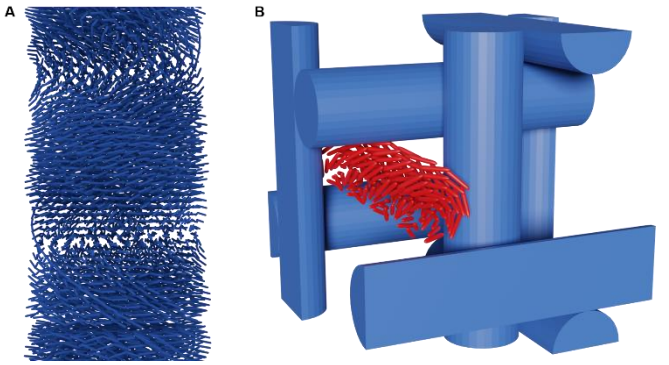

Fig. 1 Schematic representation of the structure of a chiral-nematic (A) and a body centred cubic blue phase I (BP I, B).

Recently, we reported a modular approach towards supramolecular liquid crystals, which allowed us to perform systematic structure-property relationship studies of hydrogen-bonded liquid crystals (HBLCs).[11–13] The modularity of this approach provides access to materials with the desired properties by mixing of pre-tailored building blocks, and further beneficial properties arising from the self-assembly process itself.[14–19] Recently, we employed the modular approach to induce chirality in self-assembled HBLCs and observed a variety of different chiral mesophases depending on the composition of the assemblies (Scheme 1).[20]

In our previous study eight chiral HBLCs were obtained by mixing hydrogen bond donors (phloroglucinol (**PHG**) or 1-fluorophloroglucinol (**F-PHG**)) with hydrogen bond acceptors (stilbazole (**St**) or azopyridine (**Ap**)). Systematic substitution of the HB acceptors by the chiral analogue bearing the chiral (*S*)-citronellyl alkoxy chain(**St***, **Ap***) yielded a series of assemblies displaying a variety of chiral mesophases. All investigated assemblies in our previous study had the ratio of 1:1.5:1.5 (HB donor:achiral HB acceptor:chiral HB acceptor).[20]

[a] *Institute of Organic Chemistry, University Duisburg-Essen, Universitätsstraße 7, 45141 Essen, Germany. E-mail: michael.giese@uni-due.de.*
[b] *Dipartimento di Ingegneria, Università degli Studi di Palermo, Viale delle Scienze, Ed. 6, Palermo 90128, Italy.*
[c] *Institute of Inorganic Chemistry, University Duisburg-Essen, Universitätsstraße 7, 45141 Essen, Germany.*
[d] *Department of Physics and Astronomy University of British Columbia, 6224 Agricultural Road, Vancouver, Canada*
† These authors contributed equally.

Electronic Supplementary Information (ESI) available: CIF-File; synthetic protocols; polarised optical microscopy images and differential scanning calorimetry. See DOI: 10.1039/x0xx00000x

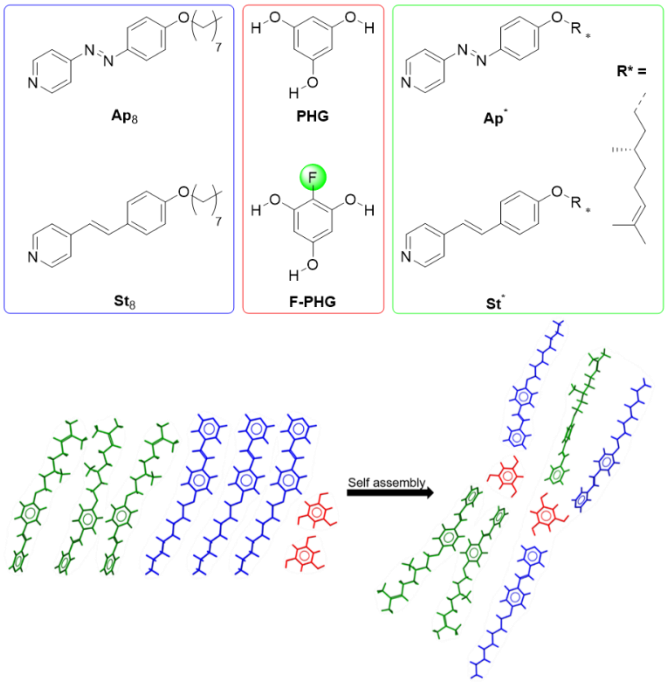

Scheme 1 Schematic representation of the modular concept for the systematic investigation of the chiral transfer in hydrogen-bonded liquid crystals.

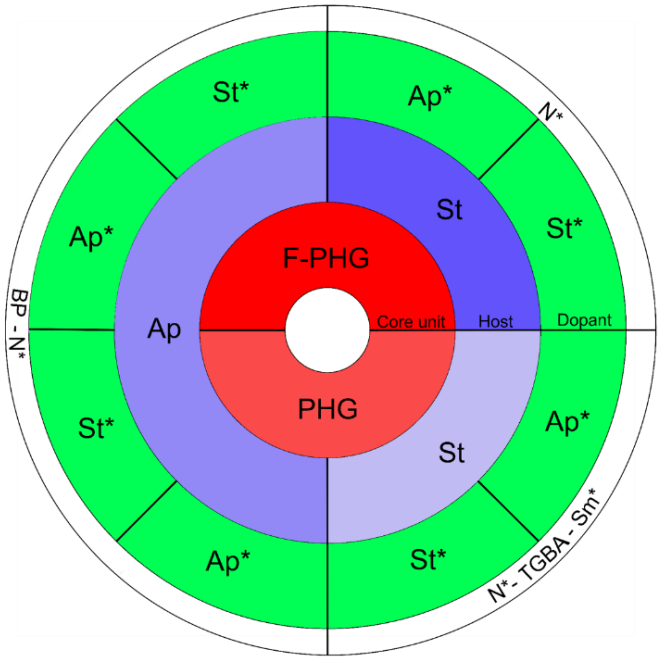

Fig. 2 Graphical summary of the results as obtained for the chiral induction in hydrogen-bonded liquid crystals. (BP for Blue Phase, N* for chiral nematic, TGBA for twist grain boundary and Sm* for chiral smectic).

As it turned out, the emerging mesophases are strongly correlated with the complex compositions and the linking group in the individual building blocks. By mixing the achiral stilbazole and the fluorinated core unit (**F-PHG**), only a chiral nematic phase arises, regardless of the chiral component (**St*** or **Ap***) of the assembly. The absence of the highly polarising fluorine atom at the core unit (**PHG**) results in a dramatic change of the mesophase sequence. Upon cooling a chiral nematic phase is followed by frustrated TGBA phase and finally a smectic phase is observed before re-crystallisation. These results are schematically shown by the right half of Figure 2. For complexes based on achiral azopyridine (see left half of Figure 2), it was found that the impact of the fluorination of the core unit has no significant influence on the mesophase sequence. In addition, it was found that upon cooling a BP-I phase with broad temperature ranges is followed by the chiral nematic phase regardless which chiral component was employed.[20]

The present study aims to understand the occurrence of different chiral phases in hydrogen-bonded liquid crystals by using a combination of computational methods and variable-temperature solid-state deuteron NMR experiments. Deuterium is chosen as a probe at the chiral chain in the chosen HBLCs.

Results and Discussion

The present manuscript aims to rationalize the differences observed in terms of chiral induction in HBLCs as previously reported by us.[20] Therefore, the reported systems were comprehensively investigated in order to rationalize the differences in the chiral induction (e.g. by variable-temperature solid-state NMR measurements (DNMR) and values for the helical twisting power values were obtained). In addition, non-chiral reference systems were investigated by complementary analytical techniques as well as computational methods and compared with the results from the chiral HBLCs.

Solid State NMR Examination of the Chiral Complexes

As mentioned in the introduction, we previously reported the chiral induction in hydrogen-bonded liquid crystals yielding a variety of chiral mesophases, including N*, BPI, Sm* and TGBA phases. Investigations using variable-temperature solid-state NMR are particularly valuable for examining chiral and achiral mesophases to provide a detailed understanding of the molecular arrangement and structural properties within a mesophase. While the structure of the BP I phase was previously investigated in detail by us using ^{19}F-NMR,[20,21] we herein report the structure of the chiral smectic (Sm*) and the twist grain boundary (TGBA) phases (Figure 3) as well as BP I by means of DNMR in two specifically ring-deuterated HBLCs.

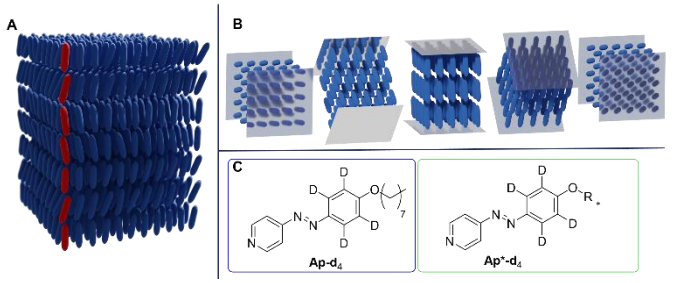

Fig. 3 Schematic representation of the structure of a chiral smectic (A) and its related twist grain boundary phase (B). Chemical structures of the ring-deuterated azopyridine derivatives (**Ap-d$_4$** and **Ap*-d$_4$**) synthesized to shed light onto the chiral induction using variable-temperature solid-sate deuteron NMR.

Therefore, the partially deuterated analogues of the chiral and the achiral azopyridines (**Ap-d$_4$** and **Ap*-d$_4$**) were synthesized and employed to create two related hydrogen-bonded assemblies, which were investigated by variable-temperature solid-state DNMR. **PHG(Ap*-d$_4$)$_{1.5}$(St-8)$_{1.5}$** shows a phase sequence: I (103 °C) ↔ N* (81 °C) ↔ TGBA (68 °C) ↔ SmA* (57 °C) ↔ Cr, and **F-PHG(Ap*-*d$_4$*)$_{1.5}$(Ap-8)$_{1.5}$** giving a sequence with a BP I phase (88 °C) ↔ BP I (83 °C) ↔ N* (62 °C) ↔ Cr, whose DNMR spectra are shown in Figure 4.

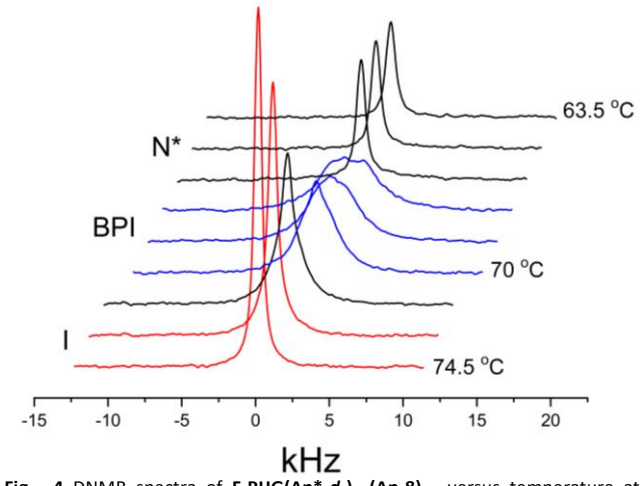

Fig. 4 DNMR spectra of **F-PHG(Ap*-*d$_4$*)$_{1.5}$(Ap-8)$_{1.5}$** versus temperature at an interval of 1.5 °C.

The BP I phase of **F-PHG(Ap*-*d$_4$*)$_{1.5}$(Ap-8)$_{1.5}$** covers a smaller temperature range (ca. 4.5 °C) compared to **F-PHG(St*)$_{1.5}$(Ap-8)$_{1.5}$** previously reported[21] and its spectra were similarly simulated (see ESI paragraph 4 for simulated spectra) using a jump model with a jump angle of 10° among 9 sites within a helix. Table 1 summarises the average quadrupole coupling $\langle \nu_q \rangle$, jump constant k_j and a Gaussian broadening factor σ in the BP I phase.

Table 1 List of fitted parameters in the BP I phase

T (°C)	$\langle \nu_q \rangle$ (kHz)	k_j (10^4 s^{-1})	σ (kHz)
70	0.2	4	7
68.5	1.45	2	7.5
67	1.5	2	5.8

In comparison with k_j of **F-PHG(St*)$_{1.5}$(Ap-8)$_{1.5}$** (ca. 0.5 MHz) the values seen in Table 1 are much smaller. This might be due in part to different sizes of jump step and/or the different chiral sites in these two cases (see HTPs below).

PHG(Ap*-*d$_4$*)$_{1.5}$(Ap-8)$_{1.5}$ shows two chiral phases and its spectra are shown in Figure 5. In the SmA* phase, a distinct quadrupolar doublet is observed from the deuterated phenyl ring, from which the order parameter can be easily determined using

$$\Delta\nu\ (kHz) = \left|\left(\frac{3S}{4}\right)\left(\frac{e^2Qq}{h}\right)(3\cos^2\theta - 1)(3\cos^2\vartheta - 1)\right| \quad (1)$$

where the quadrupolar coupling constant (e^2Qq/h) is 185 kHz, the angle ϑ between the director and the magnetic **B** field is 90°, and the angle between the C-D bond and the long axis, θ is 60 ° is assumed. The order parameter S is found as 0.55, 0.58, 0.60 and 0.62 at 58 °C, 61 °C, 64 °C, 67 °C, respectively.

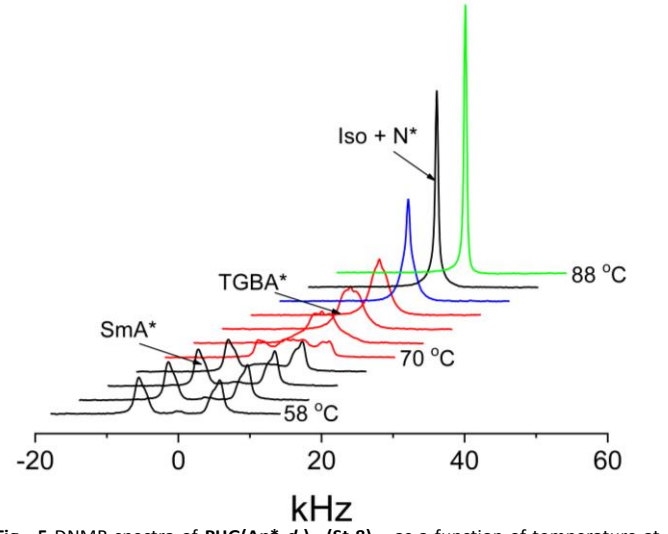

Fig. 5 DNMR spectra of **PHG(Ap*-*d$_4$*)$_{1.5}$(St-8)$_{1.5}$** as a function of temperature at an interval of 3 °C.

The TGBA spectra were simulated using the same methodology previously reported.[22] Based on the considerations of elastic and magnetic energy, the helical axes of the twisted SmA* blocks would tend to orient normal to the **B** field. The observed DNMR powder line shape reflects the above supposition, and the reorientation of the local directors among neighbouring blocks can be described by a multisite stochastic jump process with the evolution of the magnetisation for one pitch (*n* SmA* blocks) given by the Bloch-McConnell equation.[23] Figure 6 shows the simulated spectra.

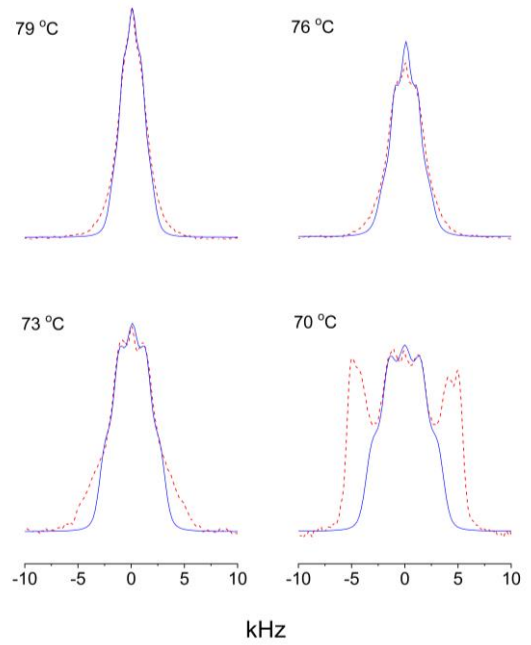

Fig. 6 Simulated TGBA spectra (black line) of **PHG**(**Ap***-d_4)$_{1.5}$(**St-8**)$_{1.5}$. Note that the experimental spectra (red line) contain features of a mixed phase.

From simulations in Figure 6, these spectra reflect a mixed phase with an increasing SmA phase component upon decreasing the temperature, and the dynamics in TGBA are determined by the kinetic parameter (k_j, jump rate) in the Bloch-McConnell equation. It was found that the jump angle between two neighbouring SmA blocks is 72° given *n* = 5, and the jump rate was found to decrease upon decreasing temperature (see Table 2). Such temperature behaviour is expected as seen in the previous work of a calamitic chiral mesogen (k_j = 7.5 x 10^3 s^{-1} at 105 °C).[22] Note that in both the BP I and the TGBA phases, the average <v_q> increases with decreasing temperature. This is normally seen due to the increasing ordering in the mesophase at lower temperatures.

Table 2 List of fitted parameters in the TGBA phase. T_2 = 100 ms.

T (°C)	<v_q> (kHz)	k_j (10^4 s^{-1})	σ (kHz)
79	2.0	1.5	1
76	2.45	1.4	1.2
73	2.87	1.1	2
70	3.4	1	2.5

The comparison of the DNMR spectra of **PHG**(**Ap***-**d$_4$**)$_{1.5}$(**St-8**)$_{1.5}$ and **F-PHG(Ap*-d$_4$)$_{1.5}$(Ap-8)$_{1.5}$** clearly indicates differences in the chiral induction. It is well known, that small variations in the molecular structure can cause a large change of the helical twisting power (HTP) and yielding different mesophases.[24] Therefore, the HTP values of the different hydrogen-bonded systems have herein been determined.

Helical Twisting Powers

The HTP is a measure for the efficiency of the chiral transfer in liquid crystalline materials. The resulting helical periodicity gives the pitch length (*P*), which is inversely proportional to the concentration of the chiral dopant (*[Dopant]*) material. The HTP depends also on the enantiomeric excess (*ee*) and follows equation (2).[25]

$$\beta = (P * [Dopant] * ee)^{-1} \quad (2)$$

The HTP values acquired in the course of this work have mainly been determined using the Grandjean-Cano-wedge cell approach.[26] Some systems have been characterised directly by measuring the pitch according to the chiral nematic-fingerprint texture due to their fluorine content and associated poor surface anchoring. Nishikawa[27] already reported a correlation between fluorination and alignment properties on treated glass. In order to understand the different chiral phases observed for the hydrogen-bonded liquid crystals reported earlier, we determined the HTP values of the chiral hydrogen-bond acceptors in different achiral host systems. We are especially interested in how the HTP values of the chiral hydrogen-bond acceptors change by variations of the achiral host system. Therefore, samples with varying concentrations between 1% and 4% of (*S*)-citronellyl-based alkoxystilbazole (**St***) and alkoxyazopyridines (**Ap***), were prepared by partial substitution of an achiral hydrogen bond acceptor by a chiral one. In the following, the measured HTP values of both the **PHG** and **F-PHG** based assemblies are summarized in Table 3 according to the core units used. The corresponding graphs can be inspected in the ESI (Figure S8).

Table 3 Experimentally evaluated helical twisting power values in μm^{-1}. The achiral host systems (PHG(Ap)$_3$ or PHG(St)$_3$) were doped by 1 – 4 mol% with the chiral acceptor moieties (*Ap** and *St**) by substitution of the corresponding achiral acceptor molecules.

Core unit	Acceptor units	HTP value [μm^{-1}]
PHG	**Ap**+*Ap**	6.2±0.2
PHG	**Ap**+*St**	5.4±0.1
PHG	**St**+*Ap**	2.7±0.1
PHG	**St**+*St**	2.8±0.2
F-PHG	**Ap**+*St**	10.6±0.4
F-PHG	**Ap**+*Ap**	5.7±0.2

By comparing the determined HTP values of the four different systems it is obvious that assemblies based on achiral **St**-hosts give significantly lower HTP values (approximately 2.7 – 2.8 μm^{-1}) compared to their **Ap**-based analogues (5.4 – 6.2 μm^{-1}). This observation is in-line with the previously reported natures of the chiral mesophases. It is well known, that blue phases are induced by dopants with a high HTP value.[28,29] In our system the BPI is exclusively observed, when the achiral azopyridine (**Ap**) is present with the chiral components possessing HTP values. Interestingly, the nature of the chiral component (**Ap***

or **St***) is less important. The achiral host systems based on stilbazole (St) form chiral smectic or TGBA phases, which is attributed to stronger interactions between the components forming the layered structures of these phases (or in other words less repulsion due to the missing free electron-pairs as seen for the azopyridine components), which may also be the reason for the lower HTP values. These findings underline the strength of our modular concept, allowing to tune the HTP values from two sides, structural changes in the chiral component or the achiral host system. For **F-PHG-St** complexes, no HTP values could be recorded due to rapid re-crystallisation and poor surface anchoring. The determined HTP values for **F-PHG-Ap** complex (Table 3) with **St*** and **Ap*** in achiral **Ap**-host systems both show HTP values higher than 5 μm^{-1}, which is again consistent with the formation of BP I phases for these assemblies. In particular, as seen in this figure the **St*** in comparison with **Ap*** in the achiral **Ap**-host systems shows a higher HTP as confirmed by the number of respective jump sites (18 versus 9) found by NMR spectral fittings.

Liquid Crystalline Behaviour of Mixed HBAs

The above results indicate the crucial role of the hydrogen bond acceptor moieties in the chiral induction. In order to understand the impact of the acceptor moieties on the nature and temperature range of the mesophase, a series of achiral hydrogen-bonded assemblies with mixed hydrogen bond acceptors (containing **Ap** and **St**) was investigated with respect to their mesophase behaviour. Therefore, five different compositions of the PHG-based assemblies (**PHG(Ap-8)$_3$**, **PHG(Ap-8)$_2$(St-8)$_1$**, **PHG(Ap-8)$_{1.5}$(St-8)$_{1.5}$**, **PHG(Ap-8)$_1$(St-8)$_2$**, **PHG(St-8)$_3$**) and the corresponding F-PHG analogues were obtained and investigated by polarized optical microscopy (POM) and differential scanning calorimetry (DSC). The results are graphically summarized in Figure 7.

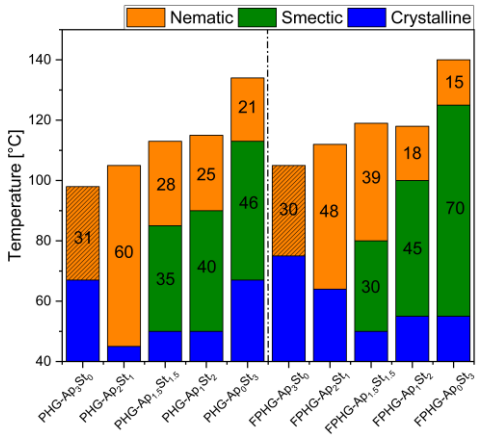

Fig. 7 Summary of transition temperatures of achiral octyloxystilbazoles (St) and octyloxyazopyridines (Ap) HBAs, derived from DSC upon heating. Crosshatched segments indicate monotropic phase behavior.

Starting with the system of **PHG(Ap-8)$_3$**, a monotropic nematic phase with a temperature range of 31 °C is obtained. Substitution of an azo moiety by a stilbazole moiety leads both to an increase in the clearing point as well as to a decrease in the re-crystallisation temperature. The temperature range of the, now enantiotropic nematic phase, thus increases to about 60 °C. The equimolar mixture in the **PHG($Ap_{1.5}St_{1.5}$)** system, yields a change in the mesophase sequence from purely nematic to nematic, followed by smectic phase upon cooling. The same phenomenon occurs as in the **PHG(Ap_1St_2)** system. The simultaneous increase in the clearing points results in a total temperature range of 63 and 65 °C, respectively. For the **PHG(St)$_3$** assembly, a drastic increase of the clearing and recrystallisation point is observed and the temperature range of the smectic phase is extended to 46 °C. **F-PHG** systems show similar trends like their non-fluorinated analogues, but exhibit a slight increase in mesophase stability. Especially the recrystallization and clearing temperatures are increased in these cases. This is reflected by consistently higher clearing temperatures compared to the non-fluorinated HBAs. Thus **F-PHG(St$_3$)** shows the highest clearing point together with the broadest smectic mesophase ($\Delta T_{Sm} \sim 70\ ^{\circ}C$). In general, the total mesophase range (nematic + smectic) increases with increasing stilbazole content, which can be attributed to the reduction of the repulsive forces between the azo-linked hydrogen bond acceptors.[30] The smectic phases start to manifest at a 1:1.5:1.5 ratio and their temperature range increases as the percentage of **St** increases. Pure azopyridine-based systems exclusively demonstrate a monotropic phase behavior. The fact that **St** are better molecules for the induction of LC phases compared to **Ap** is well known in the literature, but the reason of this behaviour has never been elucidated.[31–33] **Ap**-based HBAs are typically associated with a mainly isotropic-nematic-crystalline sequence. Mixed systems with a stilbazole content of 33% show a larger nematic phase width of up to $\Delta T_N \sim 60\ ^{\circ}C$, which can be attributed to the retardation of the clearing point and recrystallisation point caused by stilbazole.

Crystal Structure and Analysis of Intermolecular Forces

In order to correlate the mesophase behaviour of the HBAs with the underlying intermolecular forces, we have analysed the crystalline packing of related assemblies in the solid state. We are aware that there is no direct correlation between the packing of the molecules in the mesophase and their packing in the solid state. However, the identification and quantification of the non-covalent interactions in the solid state, provide useful hints on the liquid crystalline behaviour of our assemblies. Our strategy implies the use of a sophisticated technique, namely the intermolecular perturbation theory developed by Spackman,[34] and the seminal work of Gavezzotti,[34–36] as it is implemented in the *CrystalExplorer* suite.[37] This methodology recently allowed us to rationalise the aggregation-induced emission (AIE) behaviour of a series of liquid crystalline aromatic thioethers,[38,39] and to explain subtle differences in the liquid crystalline behaviour of supramolecular liquid crystals based on natural occurring polyphenols.[40] Details on the methodology are given in the ESI. A reference molecule in the crystal structure was defined (see

ESI paragraph 5 for further details) and molecular pairs (structure determinants) with surrounding molecules were analysed with respect to their intermolecular interactions. In each structure determinant, the interaction energies are calculated and split into the individual contributions of electrostatic, polarisation, dispersion and repulsion (ESI Table 1, 2 and 3, for each individual contribution). We were able to obtain co-crystals of **PHG[(Ap-8)$_x$(St-8)$_y$]** from a solution of the molecular building blocks in a mixture of acetone/acetonitrile layered with cyclohexane (see Figure 8). The exact stoichiometry could not be determined due to disorder of the bridge between the two rings in the hydrogen bond acceptor moieties (-N=N- or –CH=CH-). However, the disorder implies that there is no favoured position for stilbazoles or azopyridines in the solid state structure of the assembly. In addition, the crystal structure provides insight in the connectivity of the assembly. Taking this crystal structure as starting point we setup a series of hydrogen-bonded assemblies varying the position and ratio of azopyridine and stilbazole acceptor moieties in order to simulate the different compositions employed in the study above. The obtained model, however was well suitable as basis for quantum chemical calculations in the following.

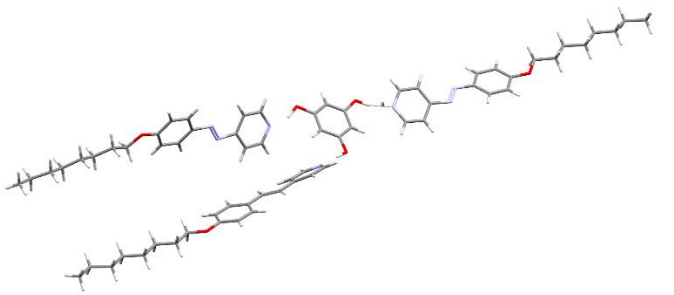

Fig. 8 Crystal structure of mixed hydrogen-bonded assembly. Disorder is omitted for clarity purposes. The assembly crystallises in the $P\bar{1}$ space group. λ-shape is perceivable. Colour chart: grey = C, white = H, red = O, blue = N.

According to the crystallographic data, the distances of the hydrogen bonds O*H*···N_{pyr} range from 1.69 Å to 1.77 Å. The two hydrogen bond acceptor molecules which are pointing in the same direction are tilted by an angle of ∠ N_{pyr}-N_{pyr} = 72.8°. The geometrical shape of the assembly resembles a λ-shape, which is in line with previous findings.[41] and the corresponding CIF-file is presented in the ESI. Since the assemblies only differ in the linking group between the two aromatic rings of the hydrogen bond acceptors, it seemed reasonable to us to generate all the possible permutations of the crystal structure of the assembly **PHG(X-8)$_3$** (X = **Ap** or **St**) to get insight in the interplay of the non-covalent forces in the assemblies. In the following our discussion will focus on the results of **PHG(Ap-8)$_3$** and the **PHG(St-8)$_3$** (Figure 9). The case of **PHG[(St-8)$_1$(Ap-8)$_2$]** is discussed in the ESI.

ARTICLE

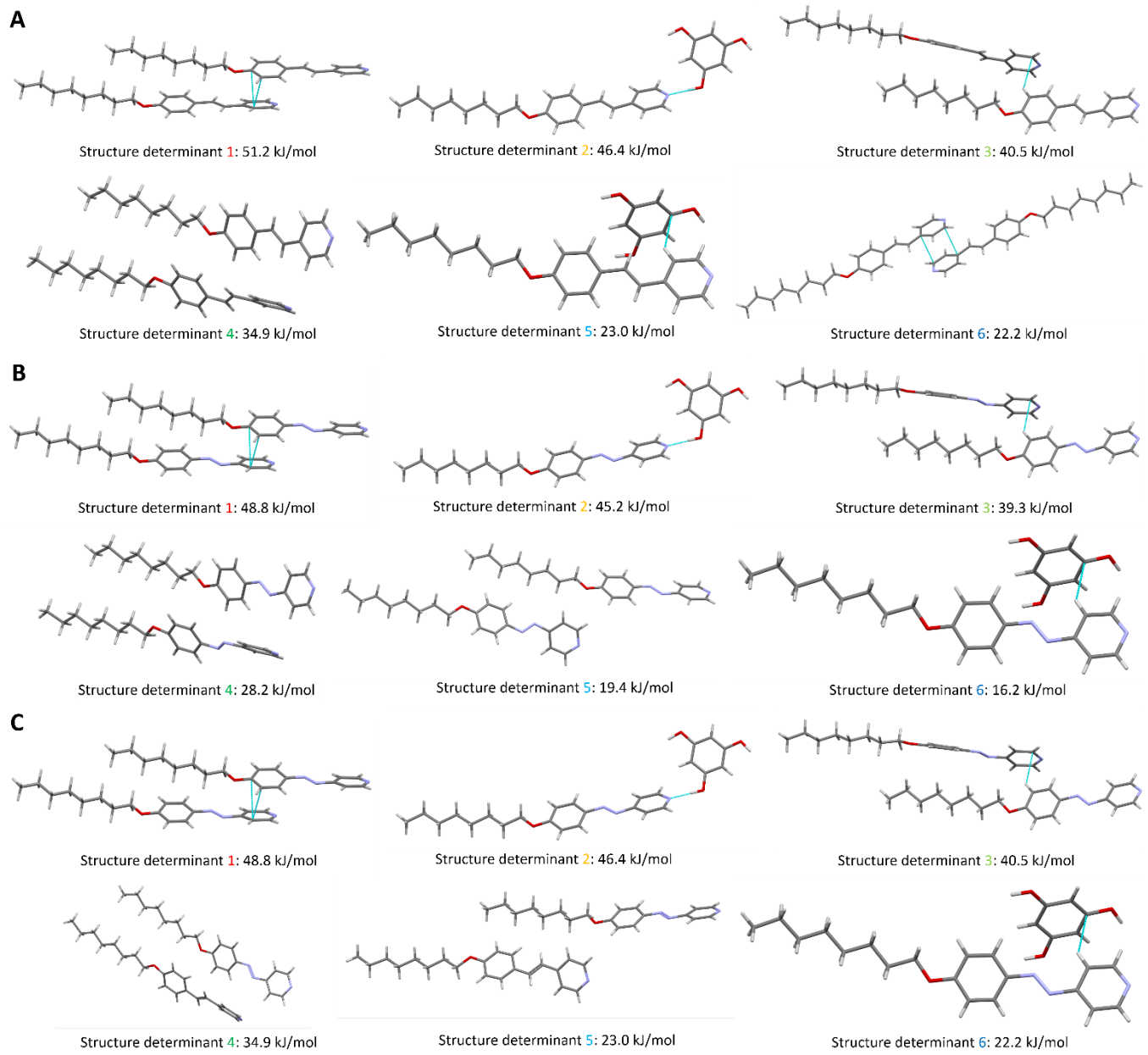

Fig. 9 Supramolecular hierarchy of the six most stabilising interactions in the **PHG(St-8)**$_3$ structure (A), **PHG(Ap-8)**$_3$ structure (B) as provided by *CrystalExplorer*. The total intermolecular energy is listed for each structure determinant, which shows parts of a pair of two interacting molecules. For each case the structure determinants are arranged in decreasing energy. Blue lines represent short intermolecular contacts below the sum of the van der Waals radii of the respective atoms. Color chart: grey = C, white = H, red = O, blue = N.

PHG(St-8)$_3$

The main contribution to the crystal packing of this assembly is the slipped stacked mode (see Structure Determinant 1), where several favourable π···π interactions between the electron rich phenyl ether ring of a stilbazole and the electron poor pyridine ring of the reference stilbazole molecule occur. This interaction mode supports the partial segregation of the aromatic cores from the aliphatic chains, giving rise to a strong interaction dominated by the dispersion contribution (table 1 ESI). The second largest contribution to the crystal packing is

given by the Structure Determinant 2, which feature a strong O*H*···N_{pyr} hydrogen bond. Usually the electrostatic contribution is dominating in the case of O*H*···N_{pyr} hydrogen bonding,[39] and this structure makes no exception, having an electrostatic contribution which is more than four times larger than the dispersive contribution (table 1 ESI). Apart from the purely dispersion bound Structure Determinant 4, the Structure Determinants 3 and 5 feature edge-to-face C*H*···π interactions which are mainly dispersion driven, but with a substantial electrostatic contribution (table 1 ESI). Structure Determinant 6 deserves a separate discussion; in this interaction mode, two stilbazole stacks with only the pyridine ring in an antiparallel fashion. This dispersion dominated interaction mode is well expected in the packing of polar mesogens.[42] Suppression of these interactions gives rise to the disruption of the LC phase.

PHG(Ap-8)$_3$

This structure features, as expected, a similar ranking of non-covalent interactions compared to the **PHG**(**St-8**)$_3$ assembly, with an important difference; namely the absence of the antiparallel stacked arrangement (former Structure Determinant 6) from the ranking of the interactions, which is substituted by a purely dispersion-driven interaction (Structure Determinant 5, Figure 9B). This difference is important to correlate the interactions occurring in our assemblies with the chiral induction of the chiral dopant chosen (see below).

PHG[(St-8)$_1$(Ap-8)$_2$]

This structure is almost identical to the former, **PHG**(**Ap-8**)$_3$ and features the same structure determinant hierarchy. They only differ in the stabilisation energies of their Structure Determinant 4 (Figures 9B and 9C). Also other small differences are present. The mixed complex features a stronger stabilisation due to the fact that the interaction between the pyridine ring and the stilbene C*H* group is stronger than the pyridine···azo interaction (see below). The Structure Determinants 6 (Figure 9B and 9C) are very similar and the ranking of interaction energies resembles the pure azopyridine-based boundary case. Accordingly, further permutations show similar behaviour and tendencies with respect to their energy ranking and type of interactions, which is why main emphasis is on the boundary cases.

Comparing the results from the structural analysis of the different assemblies shows that the intermolecular forces in the solid state are slightly stronger for the **PHG**(**St-8**)$_3$ assemblies compared to the corresponding **PHG**(**Ap-8**)$_3$ assemblies. Correlating these results with the experimental findings indicates that the interactions between the hydrogen bond acceptor moieties play a key role in the formation of the liquid crystalline phase. This is reflected by the experimental results and the observation of a smectic phase for **PHG**(**St**)$_3$, while the **PHG**(**Ap**)$_3$ assemblies exhibit exclusively a nematic phase (see Figure 7). This observation can be explained with the repulsion between the free electron pairs of the azopyridines yielding to a lower order and lower stabilities in the pure azo-driven mesophases. A comparison with the chiral systems is difficult and has to be taken with caution. However, it seems to be reasonable that the strong interaction of the stilbazole-based host systems yields smectic phases and that the "destruction" of the phase by a chiral dopant is difficult, resulting in lower HTP values and the formation of chiral smectic or TGBA phases. In contrast, the repulsion of the free electron pairs in the azopyridine-based host systems increases the structural flexibility yielding higher HTP values and mesophases of lower order (BPI and chiral-nematic phase).

Conclusions

In conclusion, we report a detailed study on chiral mesophases of hydrogen-bonded liquid crystals. The extension of our structural analysis of the chiral mesophases by variable-temperature solid-state DNMR studies clearly indicated differences in the chiral induction of the hydrogen-bonded liquid crystals. In order to quantify the chiral induction, the helical twisting powers of two chiral sidechains (**St*** and **Ap***) in different achiral host assemblies were determined by systematic substitution of the achiral component by the chiral analogue. The results of this study exhibit the nature of the achiral host system (**PHG**(**Ap**)$_3$ or **PHG**(**St**)$_3$) being controlled the HTP values. The stilbazole-based host **PHG**(**St**)$_3$ yielded significantly lower HTP values (2.7 and 2.8 μm^{-1}) compared to the azopyridine-based host **PHG**(**Ap**)$_3$ (5.4 and 6.2 μm^{-1}) and that the nature of the chiral dopant (**Ap*** or **St***) plays a minor role for the chiral induction. However, the F-PHG based complex investigated by NMR here (and before) shows a lower number of jump sites in BP I which collaborates nicely with a lower HTP value seen in Table 3 (and ESI Figure S8). In order to understand the impact of the intermolecular forces in the hydrogen-bonded assemblies on the nature of the mesophase, the phase behaviour of achiral assemblies of **PHG**(**St**)$_3$, **PHG**(**Ap**)$_3$ and the mixed systems **PHG**(**St**)$_{3-x}$(**Ap**)$_x$ were investigated and correlated to the results of a structural analysis of the assemblies in the solid state. The results indicated that the stronger interactions in **PHG**(**St**)$_3$ possess the formation of a smectic phase, while the repulsion of the free electron pairs in the **PHG**(**Ap**)$_3$ yields a nematic phase. It seems reasonable to assume that the interference of the chiral hydrogen bond acceptorwith the interactions in the achiral host systems induces different mesophases. In case of the stronger interactions in the stilbazole-based host systems the impact of the chiral acceptor unit is lower yielding lower HTP values and the formation of chiral smectic or TGBA phases. For the azopyridine-based host systems the repulsion of the free electron pairs increases the structural flexibility yielding higher HTP values and mesophases of lower order (BPI and chiral-nematic phase).

Conflicts of interest

There are no conflicts to declare.

Acknowledgements

MG gratefully thanks the Professor-Werdelmann foundation and the DFG for their granted financial support. MS acknowledges PON R&I 2014-2020 – AIM (Attraction and International Mobility), project AIM 1813040 for financial support. This work is dedicated in memory of Prof. Dr. Carsten Schmuck (*1968 - †2019).

Notes and references

1. D. J. Mulder, A. P. H. J. Schenning and C. W. M. Bastiaansen, *J. Mater. Chem. C*, 2014, **2**(33), 6695.
2. H. K. Bisoyi and Q. Li, *Acc. Chem. Res.*, 2014, **47**(10), 3184.
3. H. K. Bisoyi and Q. Li, *Angew. Chem. Int. Ed.*, 2016, **55**(9), 2994.
4. L. Wang and Q. Li, *Adv. Funct. Mater.*, 2016, **26**(1), 10.
5. E. Dubois-violette and B. Pansu, *Molecular Crystals and Liquid Crystals Incorporating Nonlinear Optics*, 1988, **165**(1), 151.
6. T. Nakagiri, H. Kodama and K. K. Kobayashi, *Phys. Rev. Lett.*, 1971, **27**(9), 564.
7. W. He, G. Pan, Z. Yang, D. Zhao, G. Niu, W. Huang, X. Yuan, J. Guo, H. Cao and H. Yang, *Adv. Mater.*, 2009, **21**(20), 2050.
8. A. Yoshizawa, *RSC Adv.*, 2013, **3**(48), 25475.
9. H.-S. Kitzerow, H. Schmid, A. Ranft, G. Heppke, R. A. M. Hikmet and J. Lub, *Liq. Cryst.*, 1993, **14**(3), 911.
10. H. Kikuchi, M. Yokota, Y. Hisakado, H. Yang and T. Kajiyama, *Nat. Mater.*, 2002, **1**(1), 64.
11. M. Pfletscher, M. Mezger and M. Giese, *Soft matter*, 2018, **14**(30), 6214.
12. M. Pfletscher, C. Wölper, J. S. Gutmann, M. Mezger and M. Giese, *Chem. Commun.*, 2016, **52**(55), 8549.
13. M. Saccone, M. Pfletscher, S. Kather, C. Wölper, C. Daniliuc, M. Mezger and M. Giese, *J. Mater. Chem. C*, 2019, **7**(28), 8643.
14. R. Walker, D. Pociecha, J. P. Abberley, A. Martinez-Felipe, D. A. Paterson, E. Forsyth, G. B. Lawrence, P. A. Henderson, J. M. D. Storey, E. Gorecka and C. T. Imrie, *Chem. Commun.*, 2018, **54**(27), 3383.
15. Z. T. Nagy, B. Heinrich, D. Guillon, J. Tomczyk, J. Stumpe and B. Donnio, *J. Mater. Chem.*, 2012, **22**(35), 18614.
16. F. Y. Fan, S. W. Culligan, J. C. Mastrangelo, D. Katsis, S. H. Chen and T. N. Blanton, *Chem. Mater.*, 2001, **13**(12), 4584.
17. S. H. Chen, H.M.P. Chen, Y. Geng, S. D. Jacobs, K. L. Marshall and T. N. Blanton, *Adv. Mater.*, 2003, **15**(13), 1061.
18. R. F. Bryan, P. Hartley and R. W. Miller, *Mol. Cryst. Liq. Cryst.*, 1980, **62**(3-4), 311.
19. M. J. Abdy, A. Murdoch and A. Martínez-Felipe, *Liq. Cryst.*, 2016, **43**(13-15), 2191.
20. M. Saccone, M. Pfletscher, E. Dautzenberg, R. Y. Dong, C. A. Michal and M. Giese, *J. Mater. Chem. C*, 2019, **7**(11), 3150.
21. R. Y. Dong, C. A. Michal, M. Saccone, M. Spengler, C. Wölper and M. Giese, *Chem. Phys. Lett.*, 2018, **710**, 39.
22. J. Zhang, V. Domenici, C. A. Veracini and R. Y. Dong, *J. Phys. Chem. B*, 2006, **110**(31), 15193.
23. H. M. McConnell, *Chem. Phys. Lett.*, 1958, **28**(3), 430.
24. H.-S. Kitzerow and C. Bahr, eds., *Chirality in Liquid Crystals*, Springer-Verlag, New York, 2001.
25. P. G. d. Gennes and J. Prost, *The physics of liquid crystals*, Clarendon Press, Oxford, 1998.
26. R. Cano, *Bulletin de la societe francaise mineralogie et de cristallographie*, 1967, **90**(3), 333.
27. D. - S. Seo, S. Kobayashi and M. Nishikawa, *Appl. Phys. Lett.*, 1992, **61**(20), 2392.
28. H.-S. Kitzerow, *ChemPhysChem*, 2006, **7**(1), 63.
29. P. P. Crooker in *Chirality in Liquid Crystals*, ed. H.-S. Kitzerow and C. Bahr, Springer-Verlag, New York, 2001, p 186.
30. M. Spengler, R. Y. Dong, C. A. Michal, M. Pfletscher and M. Giese, *J. Mater. Chem. C*, 2017, **5**(9), 2235.
31. Y. Chen, H. Yu, L. Zhang, H. Yang and Y. Lu, *Chem. Commun.*, 2014, **50**(68), 9647.
32. L. J. McAllister, C. Präsang, J. P.-W. Wong, R. J. Thatcher, A. C. Whitwood, B. Donnio, P. O'Brien, P. B. Karadakov and D. W. Bruce, *Chem. Commun.*, 2013, **49**(38), 3946.

33. M. Saccone, M. Spengler, M. Pfletscher, K. Kuntze, M. Virkki, C. Wölper, R. Gehrke, G. Jansen, P. Metrangolo, A. Priimagi and M. Giese, *Chem. Mater.*, 2019, **31**(2), 462.

34. M. J. Turner, S. Grabowsky, D. Jayatilaka and M. A. Spackman, *J. Phys. Chem. Lett.*, 2014, **5**(24), 4249.

35. A. Gavezzotti, *J. Phys. Chem. B*, 2002, **106**(16), 4145.

36. A. Gavezzotti, *J. Phys. Chem. B*, 2003, **107**(10), 2344.

37. M. J. Turner, J. J. McKinnon, S. K. Wolff, D. J. Grimwood, P. R. Spackmann, D. Jayatilaka and M. A. Spackman, *CrystalExplorer17*, University of Western Australia, 2017.

38. S. Riebe, M. Saccone, J. Stelzer, A. Sowa, C. Wölper, K. Soloviova, C. A. Strassert, M. Giese and J. Voskuhl, *Chem. Asian J.*, 2019, **14**(6), 814.

39. M. Saccone, M. Blanke, C. G. Daniliuc, H. Rekola, J. Stelzer, A. Priimagi, J. Voskuhl and M. Giese, *ACS Materials Lett.*, 2019, 589.

40. M. Blanke, J. Balszuweit, M. Saccone, C. Wölper, D. Doblas Jiménez, M. Mezger, J. Voskuhl and M. Giese, *Chem. Commun.*, 2020.

41. M. Pfletscher, J. Wysoglad, J. S. Gutmann and M. Giese, *RSC Adv.*, 2019, **9**(15), 8444.

42. D. W. Bruce in *Supramolecular Chemistry*, ed. P. A. Gale and J. W. Steed, John Wiley & Sons, Ltd, Chichester, UK, 2012, p 10071.